Fast Design Process for a Complete Machine Series applying Coupled Analytical and Numerical Simulations

Matthias Felden, Martin Hafner and Kay Hameyer
Institute of Electrical Machines – RWTH Aachen University
Schinkelstraße 4, D-52062 Aachen, Germany
E-mail: Matthias.Felden@IEM.RWTH-Aachen.de

***Abstract*—In this paper, an automated design tool and its application to the design of a complete machine series are demonstrated. The paper points out the advantages of combining analytical methods with numerical finite element (FE) methods for the efficient electrical machine design. Prototype measurements are analyzed and compared to the simulation results in order to expose the possible limitations of the proposed approach.**

I. Introduction

Nowadays electrical machine design is mainly accomplished by rapid prototyping in order to reduce the time-to-market. In recent publications [1], [2], [3], we introduced a novel, coupled analytical and numerical sizing method that combine the advantages of both, i.e. the speed of analytical methods and the accuracy of numerical methods. The design tool presented in these publications covers electromagnetic, thermal, structure dynamic and acoustic domains. In this paper, the method is applied to the design of a permanent magnet synchronous machine (PMSM) series with surface mounted magnets for industrial purposes. Therefore the analytic, numeric and coupling of both methods will be explained in detail. The description of the thermal part, on the other hand is given in [2] and will not be described here. On basis of this design, the PMSM series has been built by an electrical machine manufacturer and the simulated machine quantities were compared to detailed prototype measurements in order to validate the presented fast design process.

II. The Automated Design Process

Fig. 1 shows the proposed electromagnetic design chain. The main idea of the analytical-FE coupling is to start from a classical analytical first dimensioning of the machine [4], [5] (Section II-A), and then to iteratively adapt the parameters of the analytical model so that they match the result of the FE simulation (Section II-B). By this procedure, the aspects that are not or poorly covered by analytical approaches (e.g. leakage, complicated geometries or saturation) can be appropriately accounted by the analytical model thanks to the coupling with FE. At the end, a model is obtained that exhibits the same accuracy as the FE model, with however the short computation time of the analytical model.

The CAD modeling, finite element problem definition, the FEA solving and the post-processing are all performed automatically by the design tool so as avoid time-consuming user interactions. All machine parameters are taken from the analytical model. A post-processing after each FE simulation monitors the deviation between analytical and numerical results. If necessary, the above-mentioned feedback loop for analytical-FE coupling is initiated (Section III). This procedure results in a very accurate simulation of the machine within a short time.

A. Electromagnetic Analytical Model

The purpose of the developed analytical model is the automated computation of various types of permanent magnet synchronous machines. Several types of constructions are considered depending on the winding type, the slot shape and the magnet configuration. Distributed and concentrated windings as well as five different slot shapes are implemented in this tool. Due to the absence of rotor windings and damper circuits in PMSMs, only the voltage equations and stator flux linkage have to be considered. In the rotating coordinate system, used to yield constant mutual reactances, the following set of steady-state equations is obtained [6]:

$$V_d = R_1 \cdot I_d - X_q \cdot I_q \,, \tag{1}$$

$$V_q = R_1 \cdot I_q + X_d \cdot I_d + V_p \,, \tag{2}$$

$$T = \frac{3 \cdot p}{\omega} \cdot V_p \cdot I_q \,. \tag{3}$$

Iron losses are computed by a Steinmetz like formula

$$p_{iron} = k \cdot B^{\alpha} \,, \tag{4}$$

where the coefficients k and α are determined by loss measurements of 1.0 T and 1.5 T, generally provided by steel manufacturer for 50 Hz. On basis of the maximal air gap flux density $B_{\delta,max}$, the flux density of stator teeth B_{ts} and yoke B_y are estimated. The time-varying flux densities B_{ts} and B_y generate the following iron losses [2]

$$P_{teeth} = V_{ts} \cdot \rho \cdot p_{iron}(B_{ts}) \cdot \left(\frac{n \cdot p}{50\,\mathrm{Hz}}\right)^{1,6} \tag{5}$$

$$P_{yoke} = V_y \cdot \rho \cdot p_{iron}(B_y) \cdot \left(\frac{n \cdot p}{50\,\mathrm{Hz}}\right)^{1,6} \tag{6}$$

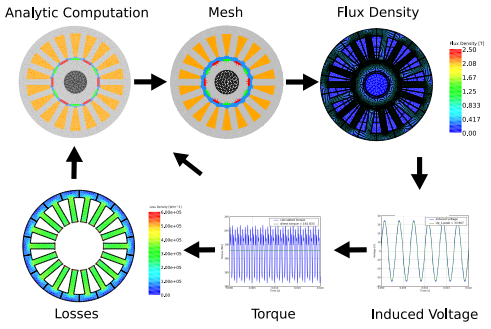

Fig. 1. Electromagnetic design chain for surface mounted PMSM.

where V_{ts} and V_y are the volumes of the corresponding stator section, ρ the mass density of the laminated steel sheets, n the rotor speed in Hz and p the number of pole pairs.

Ohmic losses P_{cu} are expressed in terms of the phase current and the winding resistance, taking end windings into account.

The mechanical losses, i.e. bearing and windage losses, are calculated, according to [7], by

$$P_{mech,Losses} = K_{mech,Losses} \cdot P_N \cdot \left(\frac{\omega}{\omega_N}\right)^2 , \qquad (7)$$

where $K_{mech,Losses}$ is a loss coefficient, close to 1% in practice. P_N is the nominal output power of the machine, ω the operation point speed and ω_N the nominal speed of the machine.

Due to axial and tangential segmentation, the eddy-current losses inside the magnets have been neglected.

B. Electromagnetic Numerical Simulation

The numerical simulation is performed with the iMOOSE package [8]. This software package offers solvers for static, transient and harmonic problems.

Iron losses are computed by means of an improved post-processing formula based on the loss-separation principle [9], [10] considering rotational hysteresis losses as well. The implemented formula assumes a separability of the iron losses (P_{Fe}) into hysteresis losses (P_h), eddy-current losses (P_{ec}) and excess losses (P_{ex})

$$P_{Fe} = P_h + P_{ec} + P_{ex} , \qquad (8)$$

where P_{ec} and P_{ex} are computed from the contributions of each harmonic of the flux density over one electrical period, whereas P_h is determined as a function of the peak value of the magnetic-flux density on the same time interval.

III. Coupling Methods

The accuracy of electromagnetic analytical models depends mainly on their ability to estimate the main electromagnetic characteristics of an electrical machine, such as the motor torque T , the mechanical power P_m and the back-emf V_p. Since these quantities are contributed in several analytic formula, they affect the whole analytic computation. The torque is given by:

$$T = \frac{P_m}{2 \cdot \pi \cdot n} \qquad (9)$$

with

$$P_m = 3 \cdot I_q \cdot V_p . \qquad (10)$$

For the back-emf, the following equation is obtained [3]:

$$V_p = \frac{1}{\sqrt{2}} \cdot \omega \cdot K_w \cdot w_{Phase} \cdot \frac{K_{geo}}{K_{\phi,\sigma}} \cdot B_{\delta,max} , \qquad (11)$$

where K_w represents the winding factor and w_{Phase} the windings per phase. The factor $K_{\phi,\sigma}$ represents the leakage flux of the permanent magnets and K_{geo} is a factor which represents the geometry of the machine. All quantities in (11) depend on fixed values like the geometry of the machine or the number of windings and their distribution, except the maximum air gap flux density. According to [4], the equation is

$$B_{\delta,max} = \sqrt{2} \cdot B_m \cdot \frac{A_{pole}}{A_{gc}} \qquad (12)$$

where B_m represents the effective magnet flux density, calculated by the remanence flux density, depending on the magnet temparature. A_{pole} describes the magnet area per pole and A_{gc} the magnetized area in the stator.

Losses are a critical factor in electrical machine design, since they significantly influence the electromagnetic material properties and hence impact the characteristics of the whole drive. Therefore, loss quantities have to be considered carefully in the analytic-FE coupling. Since the computation of copper and mechanical losses is same in both methods, only the analytic iron losses, consisting of teeth (5) and yoke (6) losses,

$$P_{iron} = P_{teeth} + P_{yoke}. \qquad (13)$$

need to be coupled.

The discrepancies between the analytical model and the FE model are accounted for in the proposed approach by introducing update coefficients in the analytical models. These factors are determined by identification of the responses of the FE model and the analytical model. After various experiments, we have found that three update coefficients were enough to reach in the end a good agreement between both models. The update rules writes as follows

$$B_{\delta,max}(i+1) = B_{\delta,max}(i) \cdot K_{B_\delta} , \qquad (14)$$

$$V_p(i+1) = V_p(i) \cdot K_{V_p} , \qquad (15)$$

$$P_{iron}(i+1) = P_{iron}(i) \cdot K_{P_{iron}} . \qquad (16)$$

with K_{B_δ}, K_{V_p} and $K_{P_{iron}}$ the update coefficients and where (i) denotes the value of a quantity of the analytical model at the ith iteration.

Methods (a), (b) and (c) below present different approaches for the determination of the update coefficients. The results are summarized in Table I, listing the deviations between the numeric and analytic method results of torque (T), voltage (V), iron losses (P) and flux density (B) for each proposed method after each iteration step. In the example given here, the deviation before a re-parameterization (i = 1) is significant with respect to torque and iron losses. Even if, B is in good agreement, the quantity V shows a slight difference.

TABLE I
DEVIATIONS BETWEEN NUMERIC (N) AND ANALYTIC (A) RESULTS FOR EVERY ITERATION AND FOR THE DIFFERENT COUPLING METHODS (A)-(C).

Iteration (i)	$\frac{T_N}{T_A}$	$\frac{V_N}{V_A}$	$\frac{P_N}{P_A}$	$\frac{B_N}{B_A}$
1	0,925	0,95	1,2	1,01
2 (a)	0,99	1,03	1,5	1,09
3 (a)	0,99	1,03	1,04	1,09
2 (b)	0,99	1,03	1,05	1,08
2 (c)	1,0	1,038	1,05	1,01

Method (a):

Equation (9)-(11) base on the analytic prediction of the air gap flux density in (12). To minimize the deviation in torque which is one of the most important machine characteristics, the updating can be performed by,

$$K_{B_\delta} = \frac{T_N}{T_A} \tag{17}$$

as proposed in [3]. As expected, the deviation of T and V_p vanished in iteration 2, but negatively affects in this case the iron loss computation. Furthermore, this shows the requirement for an additional iron loss updating. Even for a good agreement of the flux density, like in iteration 1, the iron losses had a deviation exceeding 20%. Adding a updating term for

$$K_{P_{iron}} = \frac{P_N}{P_A} \tag{18}$$

leads in iteration 3 to a sufficient overall agreement.

Method (b):

The successive updating in method (a) leads to an increase of the necessary iteration steps. In order to minimize the number of iterations, $\frac{P_N}{P_A}$ can be considered in each step. To avoid a mutal interaction between B_δ and P_{iron}, (17) and (18) are adapted by

$$K_{B_\delta} = \frac{T_N}{T_A} \tag{19}$$

$$K_{P_{iron}} = \frac{P_N}{P_A} \cdot \left(\frac{T_A}{T_N}\right)^\alpha \tag{20}$$

where α is the exponent of the iron loss approximation in (4). This improvement leads in the second iteration to comparable results with respect to method (a).

Method (c):

The trade-off in a simple updating by (17) and (19) leads, as exemplified in method (a),(b) to a mismatch of the flux density, even if this quantity is in good agreement. Since the analytic prediction of the flux density is among the four quantities T, V_p, P_{iron} and B_δ the most precise, method (a) is modified under the condition to keep B_δ unchanged. This yield to a updating of

$$K_{V_p} = \frac{T_N}{T_A} \tag{21}$$

$$K_{P_{iron}} = \frac{P_N}{P_A} \tag{22}$$

where the iron losses are directly considered as well. After iteration 2 the deviation is comparable good as after the third step with method (a).

IV. Machine Series Design Process

The validation of the presented fast design process has been done by designing a complete PMSM series. This series, consisting of five machine lines and five length variations per line, has a power range from 150 W up to 45 kW. Additional requirements are high power density, low DC link voltage, a cogging torque lower than 3% and a high efficiency over the whole speed and torque range. The limiting conditions are shaft height and stator diameter of the different machine lines.

For this design process, the presented method (c) was applied for coupling, due to it's advantage of a small number of iterations and simultaneously good results for the four essential design parameters.

During the development process several iterations and design variations were performed to meet with the specified design requirements and keep the necessary production effort on a low and comparative level. Therefore, different pole pair numbers, rotor diameters and windings configurations were analyzed.

Thereby, the advantage of the coupling pointed out. After an initial first updating of the analytic quantities by the FE simulation, the most design variations, like different rotor diameters and winding configurations, could be calculated only in the analytic domain. Additional numeric simulations, applied for continously checking of the coupling method, showed adequate results during the whole design variations. Therefore, further machines could be designed with just one initial numeric simulation for updating the analytic quantities and one additional simulation at the end of the design process for a final varification of the machine design.

Moreover ring magnets, rotor staggering and various permanent magnet (PM) shapes were considered to reduce cogging torque and occurring torque pulsation under load conditions.

In summery, some hundred different design variations have been simulated during this machine series design process. By applying the proposed automated rapid prototyping process all basic sizing steps as well as the evaluation of the additional design variations have been completed in less than two man-months, which shows the efficiency of the process.

V. Measurements

Actually, a first series has been build by an electric machine manufacturer. The thermal and electromagnetic measurements of the prototypes are ongoing (cf. Fig. 2).

The induced voltage measurement is shown in Figure 3(a). To reduce production costs the PM's are magnetized after placing them on the rotor. Even if this procedure leads to a non-uniform magnetisation, and therefore to harmonic flux deviations, both curves are in a good overall agreement. Afterwards, the no-load losses, consisting of the iron (13) and the mechanical losses (7), have been measured in motor and generator operation (cf. Fig. 3(b)). Both show a good

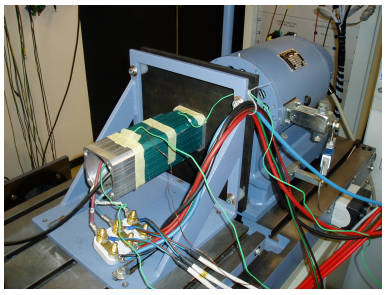

Fig. 2. Test bench for electromagnetic and thermal measurements.

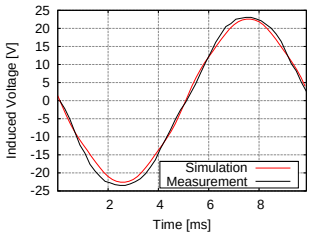

(a) Simulated and measured induced voltage at 1000 rpm.

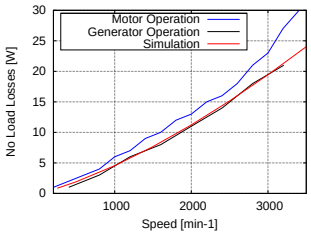

(b) Simulated and measured no load losses.

Fig. 3. Measurements of a low voltage PMSM (48V DC link) with 0.7kW rated power at 2000 rpm.

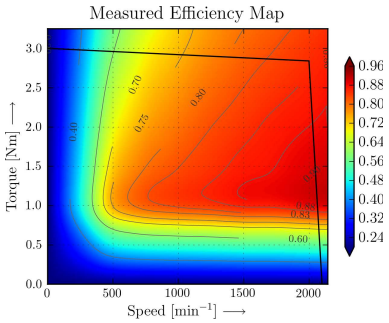

Fig. 4. Measurement of the efficiency map.

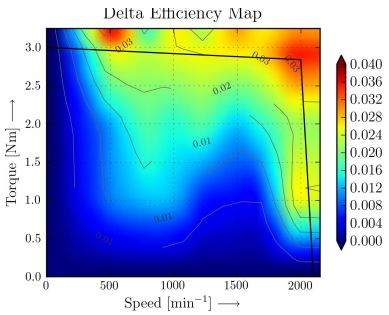

Fig. 5. Deviation between simulated and measured efficiency map.

agreement between simulations and measurements. Thereby, the motor operation leads to slightly higher losses due to the additional copper losses, caused by the "no-load current" which produces the drag torque evoked by the iron and mechanical losses. These additional copper losses in motor operation are not considered in the simulation of the no-load operation.

In a last step detailed measurements for the whole engine operating field have been realized to generate an efficiency map of the machine. The although measured temperatures show that the thermal simulation also matches quite good with the thermal measurements (Table II). Hence, the temperature depending resistances of the stator winding will match the simulated resistances and therefore the simulated and measured efficiency maps can be compared finally. Figure 5 shows the deviation between both efficiency maps, where blue areas represent really good agreement and red areas rising deviations between measurement and simulation. The Figure shows a good overall agreement but also small deviations especially for high torque and therefore high current operation points. The deviation is caused by an underestimation of the rotor magnet temperature (cf. Table II), leading to a smaller remanence flux density and consequentially to a deviation in the back-emf. According to (3) the current for the required torque and concurrently the copper losses for the high-torque operation points are a bit greater than simulated.

TABLE II
RESULTS OF THE THERMAL COMPUTATION AND MEASUREMENT FOR RATED OPERATION AND AN AVERAGE AIR TEMPERATURE OF 23 ^{o}C.

Key Temperature	**Computation** [^{o}C]	**Measurement** [^{o}C]
Frame	75	80
Endwinding	113	115
Magnet	75	78

VI. Conclusion

In this paper, a fast design process combining coupled analytical and FE simulations is presented. The coupling is done by iteratively updating the parameters of the analytical model with values extracted from the FE simulation. This enables a significant increase of accuracy of the analytical model without increasing the computation time.

The paper proposed and discussed three updating methods. Thereby, a simultaneous coupling of the back-emf and the iron losses leads to results with high correlation between analytic and FE simulations in a short time.

The design process was applied to design a complete PMSM series consisting of 25 different machines and the detailed measurements show a good overall agreement between simulations and measurements, which demonstrates the accuracy of the proposed fast design process.

References

[1] M. Schoning and K. Hameyer, "Virtual product development for electrical motors," in *IEEE International Electric Machines Drives Conference, 2007. IEMDC '07.*, vol. 2, 2007, pp. 949 –952.

[2] M. Hafner, M. Schoning, and K. Hameyer, "Automated sizing of permanent magnet synchronous machines with respect to electromagnetic and thermal aspects," in *18th International Conference on Electrical Machines, 2008. ICEM 2008.*, 2008, pp. 1 –6.

[3] M. Schoning and K. Hameyer, "Coupling of analytical and numerical methods for the electromagnetic simulation of permanent magnet synchronous machines," *COMPEL - The International Journal for Computation and Mathematics in Electrical and Electronic Engineering*, vol. 27, no. 1, no. 1, pp. 85–94, 2008.

[4] D. C. Hanselman, *Brushless Permanent Magnet Motor Design*, 2nd ed. The Writers' Collective, Mar. 2003.

[5] J. Hendershot and T. J. E. Miller, *Design of Brushless Permanent-Magnet Machines*, 2nd ed. Motor Design Books LLC, Mar. 2010.

[6] P. Vas, *Vector Control of AC Machines*. Oxford University Press, USA, Nov. 1990.

[7] J. Pyrhonen, T. Jokinen, and V. Hrabovcova, *Design of Rotating Electrical Machines*. Wiley, Feb. 2009.

[8] D. van Riesen, C. Monzel, C. Kaehler, C. Schlensok, and G. Henneberger, "iMOOSE-an open-source environment for finite-element calculations," *IEEE Transactions on Magnetics*, vol. 40, no. 2, pp. 1390–1393, 2004.

[9] G. Bertotti, A. Boglietti, M. Chiampi, D. Chiarabaglio, F. Fiorillo, and M. Lazzari, "An improved estimation of iron losses in rotating electrical machines," *IEEE Transactions on Magnetics*, vol. 27, no. 6, pp. 5007–5009, 1991.

[10] M. H. Gracia, E. Lange, and K. Hameyer, "Numerical calculation of iron losses in electrical machines with a modified Post-Processing formula," in *16th International Conference on the Computation of Electromagnetic Fields, COMPUMAG*, Aachen, Germany, Jun. 2007.